Thionyl Fluoride from Sulfur Hexafluoride Corona Discharge Decomposition: Gas-Phase Chemistry of $[SOF_2]H^+$ Ions

Federico Pepi,*,# Andreina Ricci,# Marco Di Stefano,‡ Marzio Rosi,‡ and Giuseppe D'Arcangelo†

Dipartimento di Studi di Chimica e Tecnologia delle Sostanze Biologicamente Attive, Università degli studi di Roma "La Sapienza", Piazzale Aldo Moro 5, 00185 Roma, Italy, Istituto di Scienze e Tecnologie Molecolari del CNR, c/o Dipartimento di Chimica, Università di Perugia, Via Elce di Sotto 8, 06123 Perugia, Italy, Dipartimento di Scienze e Tecnologie Chimiche, Università di Roma "Tor Vergata", Via della Ricerca Scientifica 1, 00133 Roma, Italy

Received: April 29, 2002; In Final Form: July 31, 2002

Thionyl fluoride (SOF_2) is one of the major sulfur hexafluoride (SF_6) decomposition products under electric discharges. The protonation of SOF_2 produced by corona discharge of SF_6/air mixtures has been studied by the joint application of mass-spectrometric and ab initio theoretical methods. The structurally diagnostic collisionally activated dissociation (CAD) and Fourier transform ion cyclotron resonance (FT-ICR) mass spectrometric results point to the formation of a mixed population of $[SOF_2]H^+$ protomers, the HF−SOF^+ ion−molecule complex (**II**), which reacts with selected nucleophiles as SOF^+ donor, and the covalently bounded H−OSF_2^+ species (**I**), which behaves as a protonating agent. Computational results at the B3LYP and CCSD(T) levels of theory show that the stability of isomer **I** exceeds that of **II** by 7.6 and 5.4 kcal mol^{-1}, respectively, whereas the energy barrier for their interconversion is computed to be as large as 45.2 kcal mol^{-1} at B3LYP level. The proton affinity of thionyl fluoride is estimated from FT-ICR "bracketing" experiments to be 157.7 ± 3 kcal mol^{-1}, consistent with the value obtained from theoretical calculation at B3LYP and CCSD(T) levels of theory, 153.6 ± 3 and 155.5 ± 3 kcal mol^{-1}, respectively.

Introduction

Interest in atmospheric-pressure corona discharges has increased in recent years since the development of new and more effective gas cleaning technologies based on this process. It is well-known that corona discharges cause an electrophysicochemical effect.[1−3] The electrophysical effect originates from the emission of energetic electrons, whereas ionic and radical species produced by corona discharges are responsible for the electrochemical reactions. The occurrence of these types of gas-phase reactions in the low troposphere suggests that greater attention should be devoted to atmospheric corona processes as a possible source of toxic pollutants.

On the basis of the above considerations, we have focused our attention on thionyl fluoride (SOF_2), one of the major sulfur hexafluoride (SF_6) decomposition products under electric discharges.[4−9] SF_6 is an important greenhouse gas with long (>1000 year) atmospheric residence time, of which the global world emission, approximately 5800 tons/year, is expected to rise in the future although the 1997 Kyoto conference decided that its level in the atmosphere had to be limited.[10−11] The source of SF_6 is entirely anthropogenic. The unique chemical and physical properties make this gas ideally suited to quench arcs in high-voltage electrical equipment such as circuit breakers, compact substations, and gas insulated transmission lines.[12] Additional sources of atmospheric SF_6 are the magnesium foundries, which use sulfur hexafluoride as a "cover gas" to prevent oxidation of the molten metal,[13] and the semiconductor industry, where it is used as a plasma etchant gas.[14]

In electrical equipment, SF_6 is subjected to different type of stress, essentially due to electrical discharges, that leads to its decomposition to toxic and corrosive compounds such as SF_4, rapidly hydrolyzed in air to SOF_2. Sulfur hexafluoride and its decomposition products leak to the atmosphere through imperfect seals, especially from older equipment, but most probably are also vented during testing and maintenance. Moreover, the predicted rise in tropospheric SF_6 concentration will enhance the environmental impact of its decomposition products that could also be formed in the low troposphere by lightning and corona discharge deriving from thunderstorms or high-voltage electric transmission lines or both. Owing to the intrinsic interest of SOF_2 and considering the environmental problem connected to SF_6 corona discharge decomposition, we have undertaken a comprehensive mass-spectrometric and theoretical study on the unknown ionic chemistry of $[SOF_2]H^+$ ions, aimed, in particular, to evaluate the unknown proton affinity (PA) of SOF_2, the results of which are reported herein.

Experimental Section

Thionyl fluoride was obtained both from corona discharge decomposition of SF_6 in a home-built corona discharge apparatus and from hydrolysis of SF_4. The gases used were purchased from Matheson Gas Products Inc. with a stated purity of 99.9 mol %, except for SF_4, which was obtained from Fluorochem Ltd. with a stated purity of 96.0 mol %.

Corona Discharge Reactor. The source of the corona discharge was an Edwards ST200k spark tester capable of

* To whom correspondence should be addressed. Tel: +390649913549. Fax: +390649913602. E-mail: Federico.Pepi@uniroma1.it.
# Università degli studi di Roma "La Sapienza".
‡ Università di Perugia.
† Università di Roma "Tor Vergata".

10.1021/jp021074v CCC: $22.00
Published on Web 09/18/2002

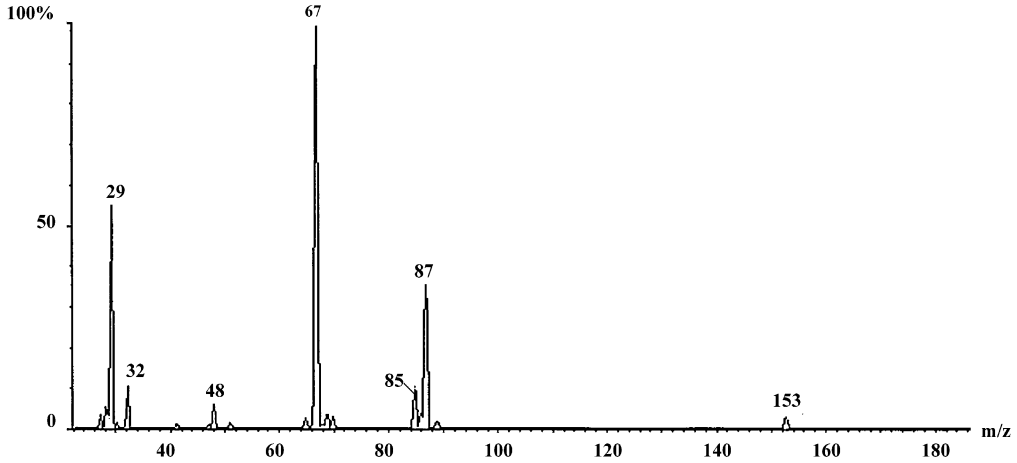

Figure 1. CH_4/CI spectrum of thionyl fluoride obtained from SF_4/H_2O mixture.

delivering a 0−50 kV pulse of 200 kHz of radio frequency. The discharge cell electrodes consist of a stainless steel cylinder and a copper wire (3.5×10^{-4} m diameter) mounted along the cylinder's central axis. The cylinder is 0.10 m long with a 3.0×10^{-3} m wall thickness and has an inside diameter of 2.5×10^{-2} m. A glass window on one side permits us to view the internal portion of the reactor to ensure that it is operating with a pure corona plasma. Two Teflon fittings are used as anchors of the central electrode on each end of the reactor. The inlet and the outlet are placed on the opposite side with respect to the glass window and were connected directly to the neural reactant gas cylinder and the mass spectrometer, respectively. Typical operating voltage of the reactor was 8−10 kV.

Mass Spectrometric Measurements. Triple quadrupole mass spectrometric experiments were performed with a model Quattro TQ instrument from VG Micromass Ltd. The ions generated in the chemical ionization (CI) source were driven into the collision cell, actually a RF-only hexapole, containing the neutral reagent. The collisionally activated dissociation (CAD) spectra were recorded utilizing Ar as the target gas at pressures up to 1×10^{-5} Torr and collision energy of 100 eV (laboratory frame). The charged products were analyzed with the third quadrupole, scanned at a frequency of 150 amu s^{-1}, accumulating about 150 scans for each run. Fourier transform ion cyclotron resonance (FT-ICR) measurements were performed using an Apex TM 47e spectrometer from Bruker Spectrospin AG equipped with an external ion source operating in CI condition. The ions generated in the external source were transferred into the resonance cell, isolated by broad band and "single shot" ejection pulses, and thermalized by collisions with Ar introduced by a pulsed valve in the cell. The pressure of the neutral reactant introduced in the cell, ranging from 1×10^{-8} to 1×10^{-7} Torr, was measured by a Bayard−Alpert ionization gauge of which the reading was corrected for the relative sensitivity to the various gases used according to standard procedures.[15] The pseudo-first-order rate constants were obtained by plotting the logarithm of the $[SOF_2]H^+_t/[SOF_2]H^+_{t=0}$ ratio as a function of the reaction time. Then, the bimolecular rate constants were determined from the number density of the neutral molecules deducted from the gas pressure. Average dipole orientation (ADO) collision rate constants, K_{ADO}, were calculated as described by Su and Bowers.[16] Reaction efficiencies are the ratio of the experimental rate constant, K_{exp}, to the collision rate constant, K_{ADO}. The uncertainty of each rate constant is estimated to be about 30%.

Computational Details. Density functional theory, using the hybrid[17] B3LYP functional[18] has been used to localize the stationary points of the investigated systems and to evaluate the vibrational frequencies. Single-point energy calculations at the optimized geometries were performed using the coupled-cluster single and double excitation method[19] with a perturbational estimate of the triple excitations approach CCSD(T).[20] Zero-point energy corrections evaluated at the B3LYP level were added to the CCSD(T) energies. The zero total energies of the species of interest were corrected to 298 K by adding translational, rotational, and vibrational contributions. The absolute entropies were calculated by using standard statistical-mechanistic procedures from scaled harmonic frequencies and moments of inertia relative to B3LYP/6-311++G(3df,3pd) optimized geometries. The 6-311++G(3df,3pd) basis set[21] has been used. All calculations were performed using Gaussian 98.[22]

Results

Formation of $[SOF_2]H^+$ Ions. Thionyl fluoride was prepared from corona discharge of 1:1 SF_6/air mixtures utilizing the apparatus described in the Experimental Section. The gaseous mixture, submitted to corona discharge processes for ca. 15 min, was directly injected into the source of the mass spectrometer through a capillary column. Thionyl fluoride was generated also from the hydrolysis of SF_4 introduced into the inlet system of the mass spectrometer in the presence of traces of water. This procedure permits elimination of all of the ionic species coming from SF_6 and air. The $[SOF_2]H^+$ ions (*m*/*z* 87) were obtained in CI/CH_4 conditions according to process 1.

$$SOF_2 + CH_5^+ \rightarrow [SOF_2]H^+ + CH_4 \qquad (1)$$

As shown by the CH_4/CI spectrum of SF_4/H_2O mixture (Figure 1), the conversion of sulfur tetrafluoride to SOF_2 is complete because no peaks deriving from SF_4 were detected. It is interesting to note the presence of the two peaks at *m*/*z* 85 and *m*/*z* 153 corresponding to the addition of SOF^+ ions (*m*/*z* 67) to water and SOF_2, respectively.

Structural Characterization of $[SOF_2]H^+$ Ions. Three different isomers of connectivity, **I**, **II**, and **III** are conceivable $[SOF_2]H^+$ product ions from reaction 1.

$$[H-OSF_2]^+ \quad \mathbf{I} \qquad [HF-SOF]^+ \quad \mathbf{II} \qquad [H-SOF_2]^+ \quad \mathbf{III}$$

Collisionally activated dissociation (CAD) mass spectrometry has been used to obtain structural information on the population of $[SOF_2]H^+$ ions from protonation of thionyl fluoride. The low-energy CAD spectrum of the ions from reaction 1, recorded at

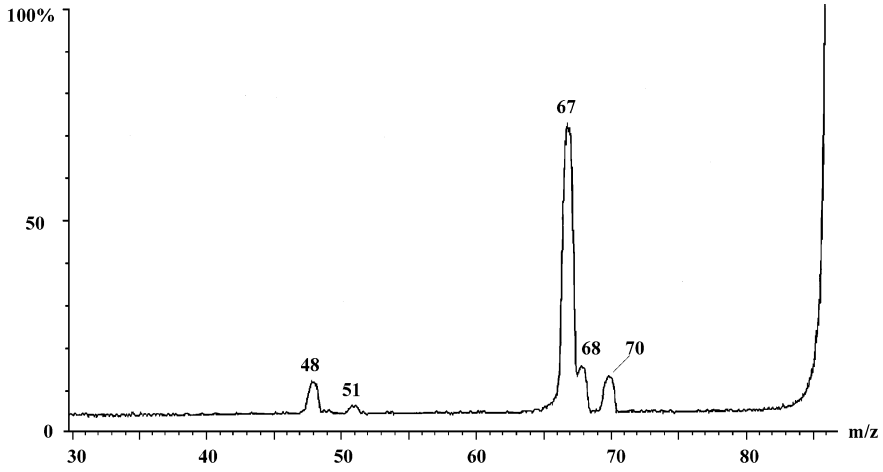

Figure 2. CAD spectrum of $[SOF_2]H^+$ ions from reaction 1.

a nominal collision energy of 100 eV (laboratory frame), is reported in Figure 2. The spectrum is dominated by the SOF^+ fragment at *m*/*z* 67, which accounts for the 75% of the whole ionic pattern, corresponding to the loss of HF, which seems to indicate a HF−SOF connectivity. By contrast, the minor fragmentation channel that leads to the ion at *m*/*z* 70 through the loss of an OH group speaks in favor of the connectivity characteristic of the isomer protonated on the oxygen atom.

Attempts at generating $H-OSF_2^+$, characterized by connectivity **I**, from the reaction of SF_3^+ ions with H_2O and subsequent loss of a HF molecule proved unsuccessful.

In the absence of model ions of known connectivity, the preliminary structurally diagnostic CAD mass spectrometry results seem to indicate the formation of a mixed population of protomers characterized both by the $H-OSF_2^+$ and the HF−SOF^+ connectivity. No evidence was obtained for the existence of a S-protonate population.

Additional structural information has been obtained by examining the reactivity of $[SOF_2]H^+$ ions by FT-ICR mass spectrometry. The $[SOF_2]H^+$ ions formed in the external CI ion source, transferred to the ICR cell and isolated after collisional thermalization by Ar, were allowed to react with selected nucleophiles introduced at low pressure into the cell.

Two main reaction channels 2 and 3 have been observed, accompanied by dissociation of the $[SOF_2]H^+$ ions into SOF^+.

$$[SOF_2]H^+ + Nu \rightarrow NuH^+ + SOF_2 \quad (2)$$

$$[SOF_2]H^+ + Nu \rightarrow NuSOF^+ + HF \quad (3)$$

Table 1 reports the proton affinities (PA) and the ionization potentials (IP) of the bases used, the experimental rate constants, and the collisional efficiencies (RE%) of the proton-transfer reaction. A representative plot of the time dependence of the abundance of all the ionic species formed from the reaction of $[SOF_2]H^+$ ions with SO_2 and CF_3CN is shown in Figure 3a,b.

When allowed to react with nucleophiles such as CH_3Cl and SO_2, the $[SOF_2]H^+$ undergoes both H^+ and SOF^+ transfer and decomposition into SOF^+. In particular, as apparent in Figure 3a, the intensity of the latter species increases during the reaction time. On the contrary, when $[SOF_2]H^+$ ions react with bases of higher proton affinity, such as CF_3CN, CF_3COOH, and CF_3CH_2OH, they undergo predominant H^+ transfer (RE = 100%), whereas SOF^+ transfer is suppressed and decomposition into SOF^+ decreases to a constant value of about 15% of the total ion intensities.

TABLE 1: ICR Reactivity of $[SOF_2]H^+$ Ions

			H^+ transfer	
nucleophile	PA (kcal mol^{-1})	IP (eV)	K_{exp} (10^{-10} cm^3 s^{-1} mol^{-1})	RE (%)
CO	142.0	14.01		
CH_3F	143.1	12.50		
CHF_3	148.1	13.86	0.394 ± 0.052	3.4
COS	150.2	11.18		
CH_3Cl	154.7	11.26	4.67[a] ± 0.67	30.7[a]
SO_2	160.7	12.34	4.29[a] ± 0.042	34.0[a]
CF_3CN	164.7	13.93	8.70 ± 0.91	100
CF_3CH_2OH	167.4	11.50	16.4 ± 0.67	100
CF_3COOH	170.1	11.50	18.0 ± 2.4	100

[a] K_{exp} and reaction efficiency including SOF^+ transfer.

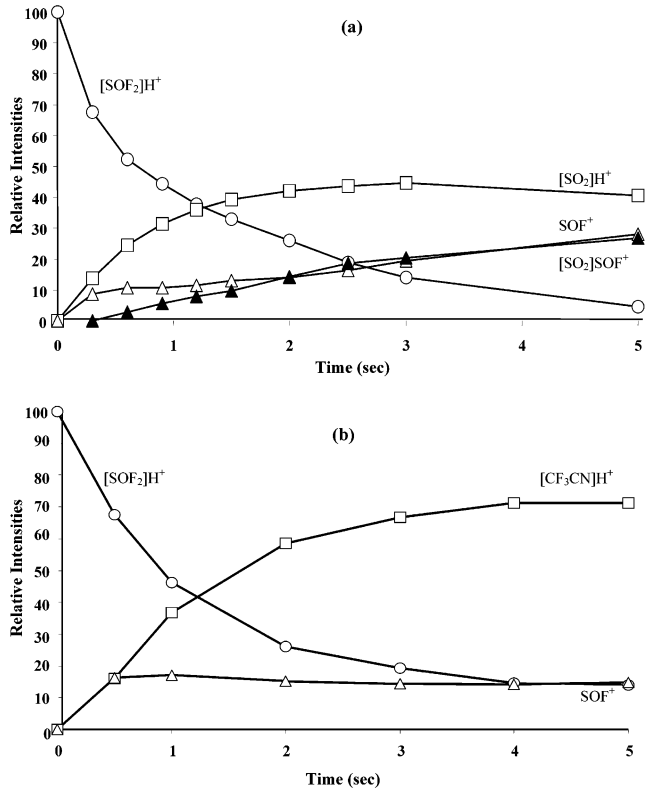

Figure 3. Time profiles of the ionic intensities in the reaction of $[SOF_2]H^+$, *m*/*z* = 87, with (a) SO_2 and (b) CF_3CN.

The efficiency of proton transfer to CHF_3 was very low, whereas no reactions were observed with bases such as CO and CH_3F characterized by a low basicity. Consistent with the

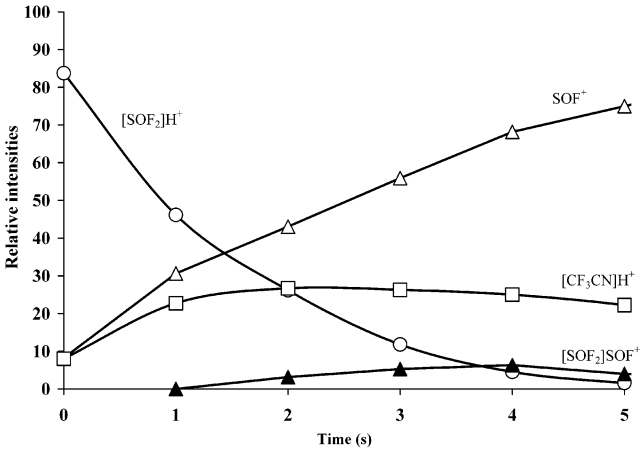

Figure 4. Time profile of the ionic intensities in the reaction of $[SOF_2]H^+$, $m/z = 87$, with a mixture of SOF_2 and CF_3CN.

relative ionization potential of the species involved, charge transfer was the only reaction channel observed with COS. However, in the absence of any other reaction channels, the abundance of SOF^+ fragment ions remains constant and lower than 15% of the total ion current.

In contrast, fragmentation into SOF^+ ions becomes the main process when $[SOF_2]H^+$ ions were allowed to react in the ICR cell with mixtures containing a nucleophile and SOF_2 itself (Figure 4). It is worth noting that under these conditions one observes the SOF^+ transfer reaction to SOF_2 yielding an ionic product of m/z 153 previously observed in the SOF_2 CH_4/CI spectrum.

These results are consistent with the expected formation of two isomeric $[SOF_2]H^+$ ions under the mass spectrometric condition used, one of which, presumably **I**, reacts as a protonating species and the other, presumably **II**, reacts as SOF^+ donor.

The PA of SOF_2. Among the methods of measuring the basicity of gaseous species, the equilibrium method presupposes the knowledge of the pressure of both neutral bases involved.[23−24] In our ICR experiments, SOF_2 was obtained from the hydrolysis of SF_4 in the presence of traces of water, which precludes the possibility of determining with any degree of accuracy its partial pressure in the ICR cell and, therefore, of using the equilibrium method. A viable alternative is provided by the "bracketing method",[22,23] which estimates the PA by measuring the efficiency of proton transfer from the investigated molecule, $[SOF_2]H^+$, to bases of known PA. For exothermic proton transfer reactions, the efficiency is high; for strongly endothermic processes, it drops to zero, whereas for reactions endothermic by no more than 1−3 kcal mol^{-1}, it is low but still measurable. As reported in Table 1, the efficiency of the proton transfer from $[SOF_2]H^+$ to CHF_3 (PA = 148.1 kcal mol^{-1}) was very low, while a 100% of efficiency was measured with bases such as CF_3CN (PA = 164.5 kcal mol^{-1}). This PA range may be restricted considering that the proton transfer was observed with both SO_2 and CH_3Cl. Therefore, it is reasonable to assume that the proton affinity of SOF_2 is intermediate between that of CH_3Cl and of SO_2, which defines a PA interval from 154.7 to 160.7 kcal mol^{-1} according to the more recent NIST database.[25] In evaluating the uncertainty range of this measurement, several sources of errors, and their propagation, need to be considered. Indeed, apart from the error attached to the tabulated PA values of the reference bases used, a significant contribution could arise from the measurement of the reaction efficiencies in the presence of competing reaction channels, such as SOF^+ transfer. However, the intensity of the SOF^+ adduct never exceeds that of the protonated base for both SO_2 and CH_3Cl. By taking into account the various sources of error, a reasonable estimate of the overall uncertainty of the experimental PA of SOF_2 is on the order of ±3 kcal mol^{-1}. Given the limited accuracy of these measurements, the PA of SOF_2 can be estimated to be 157.7 ± 3 kcal mol^{-1}.

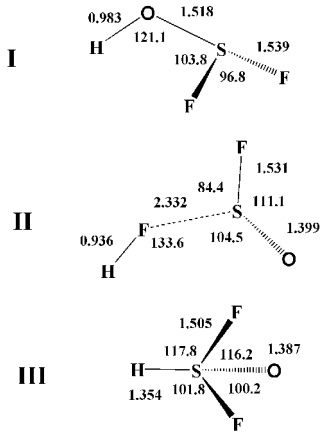

Figure 5. B3LYP/6-311++G(3df,3pd) optimized geometries of the $[SOF_2]H^+$ ions. Bond lengths are in Å and bond angles in deg.

TABLE 2: Calculated Enthalpies of Reactions and Barrier Heights at 298 K (kcal mol^{-1})

	ΔH_{298}		E_a	
	B3LYP	CCSD(T)	B3LYP	CCSD(T)
$HOSF_2^+ \rightarrow OSF_2 + H^+$	153.6	155.5		
$OSF{-}FH^+ \rightarrow OSF_2 + H^+$	146.0	150.1		
$HSOF_2^+ \rightarrow OSF_2 + H^+$	122.8	128.1		
$HOSF_2^+ \rightarrow OSF{-}FH^+$	7.6	5.4	45.2	46.0
$HOSF_2^+ \rightarrow HSOF_2^+$	30.3	27.4	75.3	75.6
$OSF{-}FH^+ \rightarrow HSOF_2^+$	22.6	22.0	70.4	74.3

Theoretical Calculations. To verify the above-mentioned experimental predictions, theoretical calculations have been performed by using an approach based on the density functional theory using the hybrid B3LYP functional. Additional calculations have also been carried out using the coupled-cluster single and double excitation method with a perturbational estimate of the triple excitations CCSD(T) approach.

Three structures, **I**, **II**, and **III**, have been found that correspond to minima on the potential energy surface of $[SOF_2]H^+$ and of which the geometrical parameters are illustrated in Figure 5. Table 2 reports the $\Delta H°_{298}$ changes relative to the protonation reaction leading to the three different isomers calculated both at B3LYP and at CCSD(T) level, together with the barrier heights for their interconversion.

Protonation at the oxygen atom of SOF_2 gives the most stable structure **I**. Comparison of the optimized structure of this protonated form with that of neutral SOF_2 [26−28] reveals that O protonation shortens the S−F bond and lengthens the S−O bond. The proton affinity at the oxygen atom of SOF_2 is computed to be 153.6 ± 3 and 155.5 ± 3 kcal mol^{-1} at the B3LYP and CCSD(T) levels of theory, respectively.

Protonation at the fluorine atoms gives rise to isomer **II**, which lies only 7.6 and 5.4 kcal mol^{-1} higher in energy than ion **I**. Considering the relatively long S−FH bond distance, 2.332 Å, with respect to that of neutral SOF_2, 1.652 Å, this ionic species can be viewed as a loosely bound ion−molecule complex between SOF^+ and HF. The interconversion between the O-protonated ion **I** and the F-protonated ion **II** requires overcoming a significant activation barrier, computed to be 45.2

kcal mol^{-1} at the B3LYP level of theory (46.0 kcal mol^{-1} at the CCSD(T) level).

Structure **III** with the proton attached to the sulfur atom lies 30.3 kcal mol^{-1} higher in energy than **I** at the B3LYP level of theory and is characterized by shorter S−F and S−O bonds with respect to the neutral molecule.

Discussion

The mutually supporting results from CAD and FT-ICR experiments point to the existence of two $[SOF_2]H^+$ protomers in the ionic population generated by protonation of thionyl fluoride. The CAD spectra display a dissociation pattern dominated by the SOF^+ ions produced by the nearly thermoneutral HF loss typical of the ion−molecule complex **II**. On the other hand, the only relevant feature of the presence of isomer **I** is the SF_2^+ fragment ion, at *m*/*z* 70, corresponding to the loss of an OH group. The results of FT-ICR reactive probing experiments provide additional convincing structural evidence. Protonation, together with a constant amount of decomposition into SOF^+, was the only reaction channel observed when the $[SOF_2]H^+$ ions were allowed to react with bases of PA higher than that of thionyl fluoride. The proton-transfer reaction can be ascribed to the ionic population characterized by the connectivity **I**, whereas the minor fragmentation channel into SOF^+ through the loss of an HF group originates from the ion−molecule complex **II**. The reduced extent of this fragmentation with respect to that observed in the CAD spectrum derives from the characteristic structure of loosely bonded complex of the latter isomer, which causes its partial depletion in the ionic population isolated in the low-pressure regime of the ICR cell. It is reasonable to assume that the less-basic isomer **II** does not have any protonating ability because more-basic nucleophiles, such as CF_3COOH, do not cause the depletion of its small fraction during the time in which the ions transferred are isolated and thermalized in the ICR cell.

Peculiar behavior was observed in the reactions of $[SOF_2]H^+$ ions with bases such as CH_3Cl and SO_2. The intensity of the SOF^+ fragment ions increases during the reaction time, and a new reaction channel, the nucleophilic displacement of a HF molecule with the formation of the SOF^+ addition products, appears. The only isomer that can be responsible for this reactivity is the kinetically unstable isomer **II**, which instantly decomposes in the low-pressure regime of the ICR cell. Therefore, assuming that a few milliseconds after the isolation the population of $[SOF_2]H^+$ ions consists of isomer **I** only, the observation of the SOF^+ adducts with those nucleophiles may conceivable derive from an intracomplex isomerization of **I** into **II** mediated by bases having a proton affinity close to the local PAs of both the oxygen and fluorine atoms of SOF_2.

$$[B\ H\text{-}OSF_2]^+ \longrightarrow [B\ HF\text{-}SOF]^+ \begin{cases} \longrightarrow SOF^+ + B + HF & (4) \\ \longrightarrow B\text{-}SOF^+ + HF & (5) \end{cases}$$

(INC1) (INC2)

A proton affinity difference of a few kcal mol^{-1} between the base B and SOF_2 enhances the lifetime of the ion−neutral complex, **INC1**, and hence may increase the possibility of the intracomplex proton transfer between B and SOF_2. Besides, although the intracomplex proton transfer from BH^+ to the less-basic fluorine atom should be unfavored enthalpically, the loss of the HF molecule may favor this process from an entropic point of view. Intracomplex isomerization of **I** into **II** leads to the formation of another ion−neutral complex, **INC2**, formed by a SOF^+ ion, the base B, and a hydrogen fluoride molecule. **INC2** may dissociate into its components (reaction 4) or lose the HF molecule (reaction 5), giving rise to the enhanced fragmentation into SOF^+ and to the SOF^+ transfer product observed in the ICR experiments.

Together with the intracomplex isomerization, an intermolecular conversion of **I** into **II** occurs in the CH_4/CI and FT-ICR experiments where the $[SOF_2]H^+$ ions can interact with SOF_2 itself. In these cases, the protomer **II** is formed by the self-protonation reaction, of which the endothermicity corresponds to the small stability difference between **I** and **II**. The predominant dissociation into SOF^+ and the appearance of the SOF^+ transfer products to bases of high PA, such as water, observed in the CH_4/CI experiments, confirm the enhanced amount of the fluorine-protonated isomer in the high-pressure mass-spectrometric conditions.

This evidence corroborates the small proton affinity difference between the oxygen and fluorine atoms of SOF_2 and the ICR bracketing results that give a PA of thionyl fluoride ranging from 154.7 (CH_3Cl) to 160.7 kcal mol^{-1} (SO_2).

The theoretical results support the conclusion, based on the mass-spectrometric evidence, for the formation of a mixed ionic population. The small difference in the calculated stability of protomers **I** and **II**, 7.6 and 5.4 kcal mol^{-1} at B3LYP and CCSD(T) levels of theory, respectively, allows the formation of both protomers from reaction 1 of which the exotermicity amounts to 27.8 kcal mol^{-1}. Moreover, the two protomers are trapped in deep potential wells because the barrier for their interconversion is computed to be as large as 45.2 kcal mol^{-1}. The theoretical structures of isomers **I** and **II**, illustrated in Figure 5, are consistent with the CAD fragmentation pathway and the observed FT-ICR reactivity. The optimized geometry of the isomer **II** characterizes this protomer as an ion−molecule complex between SOF^+ and HF with a large separation, 2.332 Å. The relatively weak coordination of the monomers explains the extensive fragmentation into SOF^+ observed in the CAD spectra and the SOF^+ donor ability of **II**, with the occurrence of simple ligand-exchange reactions, shown in CI and ICR condition. By contrast, the optimized structure of the most stable isomer **I** characterizes this ion as a protonating species, consistent with the FT-ICR reactivity of the ionic population cooled by collisions with Ar.

Comparison between the 153.6 ± 3 and 155.5 ± 3 kcal mol^{-1} PA values of SOF_2, computed at the B3LYP and CCSD(T) level of theory, respectively, and the experimental value of 157.7 ± 3 kcal mol^{-1} reveals a discrepancy of 2−4 kcal mol^{-1}, which however is not large if one considers the uncertainty ranges of the two sets of results. By combining the experimental PA of SOF_2 with the theoretically computed difference between its gas-phase basicity (GB) and PA, one obtains a GB of SOF_2 = 149.9 ± 3 kcal mol^{-1} and, from available thermochemical data, a heat of formation of $H-OSF_2^+$ cations of 78 ± 3 kcal mol^{-1}.

Conclusions

Thionyl fluoride is one of the major products obtained from sulfur hexafluoride in corona discharge processes. The relevance of this molecule to atmospheric chemistry derives from the possibility that atmospheric SF_6, of which the global world emission is continuously rising, may generate toxic pollutants, such as SOF_2, in the corona discharge promoted by high-voltage power lines or by thunderstorms. Experimental and theoretical studies of the protonation reaction of SOF_2 provides strong evidence for the existence of both oxygen- and fluorine-protonated isomers as two distinct species in the gas phase. The

more stable isomer **I** is characterized by the connectivity $H-OSF_2^+$ and, accordingly, behaves in FT-ICR conditions as Brønsted acid undergoing exclusively H^+ transfer to selected bases. In this context, application of theoretical and experimental methods allowed evaluation of the unknown PA of thionyl fluoride, of which the best theoretical estimate, 155.5 ± 3 kcal mol^{-1} at the CCSD(T) level, is comparable with the experimental one, 157.7 ± 3 kcal mol^{-1}, obtained utilizing the FT-ICR "bracketing" method. On the other hand, consistent with its connectivity, the fluorine-protonated isomer **II**, which can be viewed as a loosely bounded ion−molecule complex $HF-SOF^+$, easily decomposes into HF and SOF^+ and, if generated by a reaction less exothermic than reaction 1 and stabilized by multiple collisions, may act as SOF^+ donor.

Acknowledgment. The authors express their gratitude to Prof. Fulvio Cacace and Prof. Antonio Sgamellotti for encouragement and helpful discussions. Work carried out with the financial support of the Universities of Rome "La Sapienza" and "Tor Vergata", University of Perugia and Consiglio Nazionale delle Ricerche (CNR).

References and Notes

(1) Chakrabarti, A.; Mizuno, A.; Shimizu, K.; Matsuoka, T.; Furuta, S. *IEEE Trans. Ind. Appl.* **1995**, *3*, 500.

(2) Yamamoto, T.; Ramanathan, K.; Lawless, P. A.; Ensor, D. S.; Newsome, J. R.; Planks, N.; Ramsey, G. H. *IEEE Trans. Ind. Appl.* **1992**, *28*, 528.

(3) Moon, J. D.; Kim, J. K.; Lee, D. H. *IEEE Trans. Ind. Appl.* **1998**, *34*, 1212.

(4) Sauers, I.; Harman, G. *J. Phys. D: Appl. Phys.* **1992**, *25*, 761.

(5) Coll, I.; Casanovas, A. M.; Vial, L.; Gleizes, A.; Casanovas, J. *J. Phys. D: Appl. Phys.* **2000**, *33*, 221.

(6) Coll, I.; Casanovas, A. M.; Vial, L.; Gleizes, A.; Casanovas, J. *J. Phys. D: Appl. Phys.* **2000**, *33*, 1348.

(7) Vial, L.; Casanovas, A. M.; Coll, I.; Casanovas, J. *J. Phys. D: Appl. Phys.* **1999**, *32*, 1681.

(8) Belarbi, A.; Pradayrol, C.; Casanovas, A. M.; Casanovas, J. *J. Appl. Phys.* **1995**, *77*, 1398.

(9) Kurte, R.; Heise, H. M.; Klockow, D. *J. Mol. Struct.* **2001**, *565−566*, 505.

(10) Maiss, M.; Steele, L. P.; Francey, R. J.; Fraser, P. J.; Langenfelds, R. L.; Trivett, N. B. A.; Levin I. *Atmos. Environ.* **1996**, *30*, 1621.

(11) Victor, D. G.; Macdonald, G. J. *Clim. Change* **1999**, *42*, 633.

(12) Sauers, I.; Ellis, H. W.; Christophourou, L. G. *IEEE Trans. Electr. Insul.* **1986**, *EI21*, 111.

(13) Schemm, G.; Hanover, G. *Giesserei* **1971**, *58*, 558.

(14) Cob, J. W. *Plasma Chem. Plasma Process.* **1982**, *2*, 1.

(15) Bartmess, J. E.; Georgiadis, R. M. *Vacuum* **1983**, *33*, 149.

(16) Su, T.; Bowers, M. T. *Int. J. Mass Spectrom. Ion Phys.* **1973**, *12*, 347.

(17) Becke, A. D. *J. Chem. Phys*. **1993**, *98*, 5648.

(18) Stevens, P. J.; Devlin, F. J.; Chabalowski, C. F.; Frisch, M. J. *J. Chem. Phys*. **1994**, *98*, 11623.

(19) Bartlett, R. J. *Annu. Rev. Phys. Chem.* **1981**, *32*, 359.

(20) Raghavachari, K.; Trucks, G. W.; Pople, J. A.; Head-Gordon, M. *Chem. Phys. Lett*. **1989**, *157*, 479.

(21) (a) McLean, A. D.; Chandler, G. S. *J. Chem. Phys*. **1980**, *72*, 5639. (b) Krishman, R.; Binkley, J. S.; Seeger, R.; Pople, J. A. *J. Chem. Phys*. **1980**, *72*, 650. (c) Clark, T.; Chandrasekhar, J.; Spitznagel, G. W.; Scleyer, P. v. R *J. Comput. Chem.* **1983**, *4*, 294.; (d) Frisch, M. J.; Pople J. A.; Binkley, J. S. *J. Chem. Phys*. **1984**, *80*, 3265 and references therein.

(22) Frisch, M. J.; Trucks, G. W.; Schlegel, H. B.; Scuseria, G. E.; Robb, M. A.; Cheeseman, J. R.; Zakrzewski, V. G.; Montgomery, J. A., Jr.; Stratmann, R. E.; Burant, J. C.; Dapprich, S.; Millam, J. M.; Daniels, A. D.; Kudin, K. N.; Strain, M. C.; Farkas, O.; Tomasi, J.; Barone, V.; Cossi, M.; Cammi, R.; Mennucci, B.; Pomelli, C.; Adamo, C.; Clifford, S.; Ochterski, J.; Petersson, G. A.; Ayala, P. Y.; Cui, Q.; Morokuma, K.; Malick, D. K.; Rabuck, A. D.; Raghavachari, K.; Foresman, J. B.; Cioslowski, J.; Ortiz, J. V.; Stefanov, B. B.; Liu, G.; Liashenko, A.; Piskorz, P.; Komaromi, I.; Gomperts, R.; Martin, R. L.; Fox, D. J.; Keith, T.; Al-Laham, M. A.; Peng, C. Y.; Nanayakkara, A.; Gonzalez, C.; Challacombe, M.; Gill, P. M. W.; Johnson, B. G.; Chen, W.; Wong, M. W.; Andres, J. L.; Head-Gordon, M.; Replogle, E. S.; Pople, J. A. *Gaussian 98*, revision A.7; Gaussian, Inc.: Pittsburgh, PA, 1998.

(23) Lias, S. G.; Liebman, J. F.; Levin, R. D. *J. Phys. Chem. Ref. Data* **1984**, *13*, 695.

(24) Lias, S. G.; Batmess, J. E.; Liebman, J. F.; Holmes, J. H.; Levin, R. D.; Mallard, W. G. *J. Phys. Chem. Ref. Data* **1998**, *17*, Suppl. 1.

(25) NIST Chemistry WebBook; NIST standard Reference Database No 69, February **2000** release; data collection of the National Institute of Standards and Technology (http://webbook.nist.gov).

(26) Jursic, B. S. *J. Mol. Struct.* **1997**, *389*, 75.

(27) Cunningham, T. P.; Cooper, D. L.; Gerratt, J.; Karadakov, J.; Raimondi J. *J. Chem. Soc., Faraday Trans.* **1997**, *93*, 2247.

(28) Dobado, J. A.; Martinez-Garcia, H.; Molina, J. M.; Sundberg, M. R. *J. Am. Chem. Soc.* **1999**, *121*, 3156.